STRUCTURAL BIOLOGY

Structural basis for motilin and erythromycin recognition by motilin receptor

Chongzhao You[1,2]†, Yumu Zhang[3]†, Youwei Xu[1]†, Peiyu Xu[1]‡, Zhen Li[4], Huadong Li[3], Sijie Huang[1]§, Zecai Chen[1,2], Jingru Li[4], H. Eric Xu[1,2,3,4,5]*, Yi Jiang[3,5]*

Motilin is an endogenous peptide hormone almost exclusively expressed in the human gastrointestinal (GI) tract. It activates the motilin receptor (MTLR), a class A G protein–coupled receptor (GPCR), and stimulates GI motility. To our knowledge, MTLR is the first GPCR reported to be activated by macrolide antibiotics, such as erythromycin. It has attracted extensive attention as a potential drug target for GI disorders. We report two structures of G_q-coupled human MTLR bound to motilin and erythromycin. Our structures reveal the recognition mechanism of both ligands and explain the specificity of motilin and ghrelin, a related gut peptide hormone, for their respective receptors. These structures also provide the basis for understanding the different recognition modes of erythromycin by MTLR and ribosome. These findings provide a framework for understanding the physiological regulation of MTLR and guiding drug design targeting MTLR for the treatment of GI motility disorders.

INTRODUCTION

Human motilin is a 22–amino acid endogenous peptide that was originally isolated from porcine duodenal mucosa (1). Motilin is almost exclusively expressed in the gastrointestinal (GI) tract and shows a potent GI tract motility activity (Fig. 1A). It is involved in the regulation of the migrating motor complex, which, in turn, controls food digestion, the transmission of hunger signals, and GI hormone secretion (2, 3). The N and C termini of motilin are highly conserved across species (Fig. 1B), indicating the involvement of both termini in the physiological function of motilin (3). The human motilin receptor (MTLR) belongs to class A G protein–coupled receptors (GPCRs) and is the native receptor for motilin (4). Motilin is active in most mammals but does not respond in rodents, in which the genes of motilin and its receptor have become pseudogenes (5–7). Upon stimulation, MTLR predominantly activates the $G_{q/11}$ protein, induces Ca^{2+} fluxes, and regulates human GI motility (3, 8). Unlike motilin, the mRNA of MTLR shows a more extensive distribution in the thyroid gland, bone marrow, GI tract, brain, and retina (www.proteinatlas.org/ENSG00000102539-MLNR/tissue), indicating its multiple physiological functions (2). At present, the importance of motilin and its receptor system in regulating GI tract and hunger signaling has attracted extensive interests in designing drugs for the treatment of obesity, GI disorders, and diabetes (2, 8).

As early as the 1980s, the macrolide antibiotic erythromycin was found to mimic exogenous motilin in GI contractile activity (9, 10) and was further identified as an agonist for MTLR (11). It is structurally unrelated to motilin and shows a weaker MTLR activation ability than motilin (~1000-fold) (4). Erythromycin targets the bacterial ribosome and cell wall to achieve their bactericidal effects (12). Besides the therapeutic effects on respiratory tract infections, skin infections, chlamydia infections, pelvic inflammatory disease, and syphilis (13), long-term use of macrolides, such as erythromycin (11, 14) and azithromycin (4, 15), often causes unexpected GI disturbances, which were attributed to their off-target effects on MTLR (16, 17). Conversely, the prokinetic activity of erythromycin makes it an effective treatment for gastroparesis (14, 15). Until now, the issue of how MTLR is activated by erythromycin remains to be addressed.

Compared with other gastroparesis prokinetic medications, such as dopamine D2 receptor antagonists and 5-hydroxytryptamine receptor 4 agonists, MTLR agonists are more efficacious in improving gastric motility and limited adverse effects (18, 19). A series of motilin analogs (20, 21), macrolide derivatives (22, 23), and nonmacrolide small molecular ligands have been developed (24–26). The development of MTLR-targeted drugs will benefit from the mechanistic elaboration of the ligand recognition by MTLR. Here, we report two cryo–electron microscopy (cryo-EM) structures of the G_q-coupled MTLR bound to motilin and erythromycin. Combined with functional analysis, these structures provide insights into ligand recognition of motilin and erythromycin and the distinct modes of erythromycin recognition by MTLR and ribosome. Our findings also clarify the peptide selectivity between MTLR and ghrelin receptor (GHSR), a receptor with high sequence similarity with MTLR, and summarize the common activation mechanism of MTLR-related subfamily, which may enhance our comprehension of peptide GPCRs.

RESULTS

Overall structures of MTLR signaling complexes

To facilitate the expression of MTLR complexes, we introduced a cytochrome b562 RIL (BRIL) at the N terminus of the wild-type (WT) full-length receptor. The MTLR-G_q chimera complexes were further stabilized by the application of the NanoBiT strategy,

[1]State Key Laboratory of Drug Research, Shanghai Institute of Materia Medica, Chinese Academy of Sciences, Shanghai 201203, China. [2]University of Chinese Academy of Sciences, Beijing 100049, China. [3]School of Life Science and Technology, ShanghaiTech University, Shanghai 201210, China. [4]School of Chinese Materia Medica, Nanjing University of Chinese Medicine, Nanjing, China. [5]Lingang Laboratory, Shanghai 200031, China.
†These authors contributed equally to this work.
‡Present address: McGovern Institute for Brain Research, Massachusetts Institute of Technology, Cambridge, MA, USA.
§Present address: Department of Pharmaceutical Chemistry, University of California, San Francisco, San Francisco, CA, USA.
*Corresponding author. Email: eric.xu@simm.ac.cn (H.E.X.); yjiang@lglab.ac.cn (Y.J.)
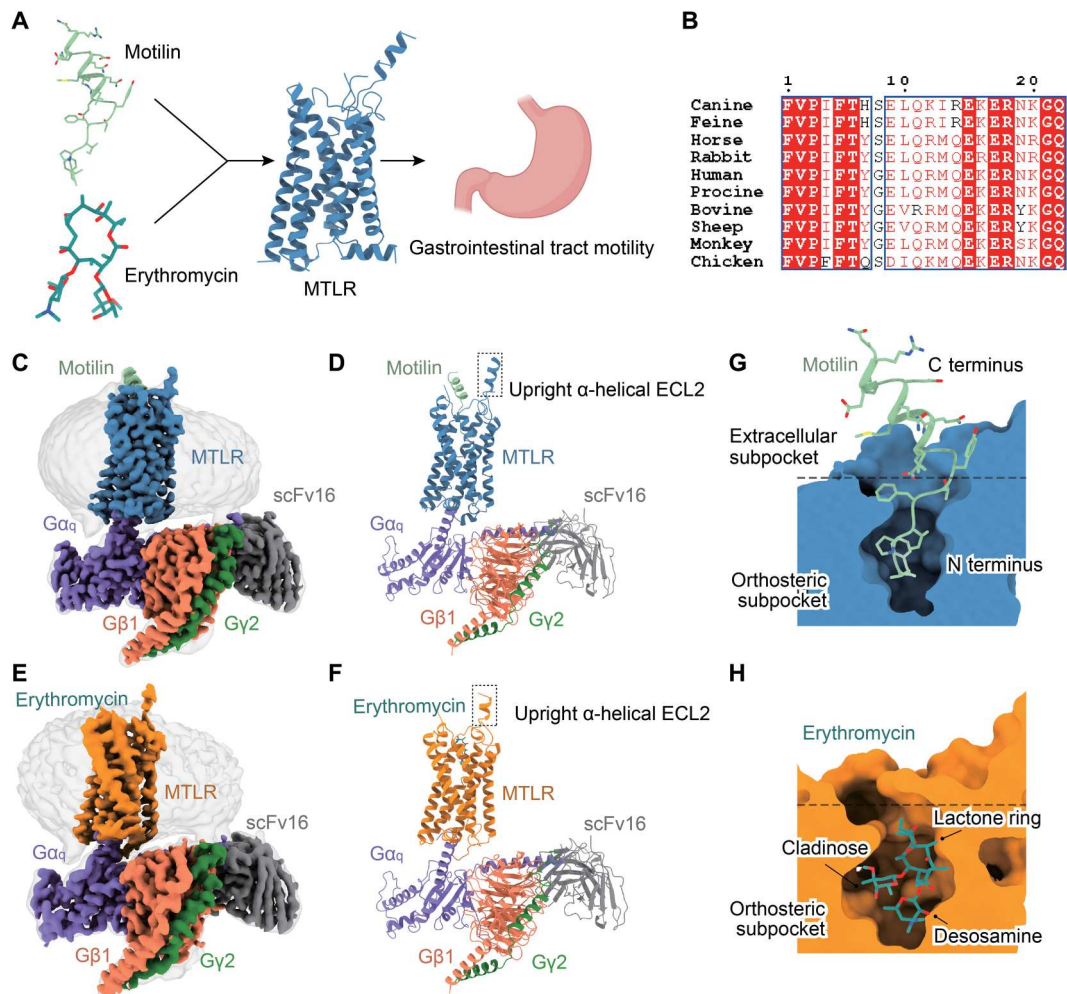
Fig. 1. Overall structures of G$_q$-coupled MTLR complexes bound to motilin and erythromycin. (**A**) Schematic illustration of ligands of MTLR and physiological effects of MTLR. (**B**) Sequence alignment of motilin across different species, created using CLUSTALW (www.genome.jp/tools-bin/clustalw) and ESPript 3.0 (https://espript.ibcp.fr/ESPript/cgi-bin/ESPript.cgi). (**C** to **F**) Orthogonal views of the density maps and models of motilin-MTLR-G$_q$-scFv16 (C and D) and erythromycin-MTLR-G$_q$-scFv16 complexes (E and F). Motilin is shown in dark green, and motilin-bound MTLR is in blue. Erythromycin is displayed in dark cyan, and erythromycin-bound MTLR is in dark orange. The G$_q$ heterotrimer is colored by subunits. Gα$_q$, purple; Gβ$_1$, coral; Gγ$_2$, green; scFv16, gray. (**G** and **H**) Cut-away view of binding subpockets of MTLR for motilin (G) and erythromycin (H).

which has been applied in the structure study of GPCR complexes (*27*, *28*). The Gα$_q$ chimera was generated on the basis of a scaffold of the mini Gα$_s$ with its N terminus replaced by corresponding sequences of Gα$_{i1}$ to facilitate the binding of scFv16 (*29*, *30*). This Gα$_q$ chimera has been used in the structure determination of the GHSR-G$_q$ protein and the bradykinin receptor–G$_q$ proteins (*31*–*33*). Unless otherwise stated, G$_q$ refers to the G$_q$ chimera, which was used for our structural studies. Incubation of motilin or erythromycin with membranes from cells coexpressing receptors and heterotrimer G$_q$ proteins in the presence of scFv16 enables effective assembly of motilin/erythromycin-MTLR-G$_q$ complexes, which produces high homogenous complex samples for structural studies.

The structures of the motilin-MTLR-G$_q$-scFv16 and erythromycin-MTLR-G$_q$-scFv16 complexes were determined by cryo-EM to the resolution of 3.2 and 3.5 Å, respectively (Fig. 1, C to F; figs. S1 to S3; and table S1). The ligand, receptor, and heterotrimeric G protein subunits are clearly visible in the EM maps (fig. S4).

The well-defined density allows accurate modeling of side chains of most residues except for the extracellular loop 2 (ECL2) segments from P183^{ECL2} to P219^{ECL2}, indicative of the high flexibility of this region (Fig. 1, C to F). Hence, these structures provide detailed information on the binding interface between ligands and MTLR, as well as the coupling interface between receptors and G$_q$ heterotrimer.

Upon binding by motilin and erythromycin, MTLR shows similar overall conformation with a root mean square deviation (RMSD) at 0.774 Å. The ECL2 segment from S220^{ECL2} to F231^{ECL2} constitutes a unique upright α helix, which is consistent with that in AlphaFold 2–predicted model (Fig. 1, D and F, and fig. S5) (*34*). This unique upright α helix ensembles an "umbrella shaft" to support the ECL2 as an "umbrella canopy" (residues 183 to 219; fig. S5), which partly contributes to motilin activity (fig. S6D) (*35*). In addition, MTLR recognizes both ligands in distinct binding modes. The motilin-binding pocket in MTLR can be divided into

two subpockets: the orthosteric subpocket in the transmembrane domain (TMD) core and the extracellular subpocket constituted by ECLs and the receptor N terminus (Fig. 1, G and H). Motilin occupies both subpockets (Fig. 1G), while erythromycin only engages the orthosteric one (Fig. 1H), which is consistent with previous reports (16, 17, 35).

Recognition of endogenous motilin by MTLR

The N terminus of motilin inserts deeply into the orthosteric subpocket in the TMD core (Fig. 1G). An extensive hydrophobic network exists between the hydrophobic pentapeptide at the extreme N terminus of motilin (F^{1M}-F^{5M}) and the residues in the orthosteric subpocket (Fig. 2, A and B). The aromatic phenyl ring of F^{1M} stretches upward and forms a hydrophobic network with $L115^{3.29}$, $F173^{4.60}$, $P237^{ECL2}$, $L245^{5.36}$, and $F314^{6.51}$. Besides hydrophobic interactions, the backbone of F^{1M} forms polar interactions with $E119^{3.33}$ and $R318^{6.55}$ (Fig. 2A). Previous findings confirmed that the positive charge of the N-terminal amino group of motilin is critical for interacting with $E119^{3.33}$. Acetylation and trimethylation of the N-terminal amine, which removed the positive charge of motilin, decreased the potency of MTLR (16). Mutating residues interacting with F^{1M}, such as $E119^{3.33}$, $F173^{4.60}$, and $R318^{6.55}$, to alanine almost abolished motilin activity, while the $L115^{3.29}$A mutant showed increased motilin activity (fig. S6, C to E, and table S2). These results indicate the critical role of the N-terminal phenylalanine, which is consistent with the previous finding that truncation of F^{1M} led to an ~280-fold decrease in peptide activity (4). Besides, F^{1M} forms an intramolecular hydrophobic contact with V^{2M} and a π-π stacking with P^{3M} (Fig. 2A). Replacing P^{3M} with phenylalanine decreased the MTLR activation potency and transferred the motilin analog to a partial agonist (20), indicative of the critical role of the residue at position 3 in determining peptide potency. In addition, I^4 and F^5 of motilin are surrounded by hydrophobic residues $F33^{NT}$, $Y321^{6.58}$, and $I338^{7.36}$ (Fig. 2B). The fact that the N-terminal segment of motilin binds to the

orthosteric subpocket and activates the MTLR (4) is consistent with the erythromycin data showing that occupying this subpocket somehow results in receptor activation.

The C terminus of motilin from T^{6M} to N^{19M} assembles into an α helix, which engages residues in the extracellular subpocket (Fig. 1G). The hydroxyl group of T^{6M} interacts with $R236^{ECL2}$ through hydrogen bond interactions (Fig. 2C). The side chains of Y^{7M} and L^{10M} make hydrophobic contacts with the receptor N terminus residues $P32^{NT}$ and $C30^{NT}$, which substantially contribute to motilin activity (Fig. 2D and fig. S6A). The side chains of R^{12M} and $D182^{ECL2}$ are within the distance of the salt bridge (Fig. 2E). The importance of the R^{12M}-$D182^{ECL2}$ salt bridge is supported by the deleterious potency of motilin on MTLR with D182A mutation (fig. S6D) and is also in agreement with a previous finding that motilin analog [1-12] showed a 158-fold increased binding affinity compared with analog [1-11] (4). The remaining aminoacids, including M^{13M}, Q^{14M}, and E^{17M}, interact with $C30^{NT}$ and $M330^{7.28}$ (Fig. 2F).
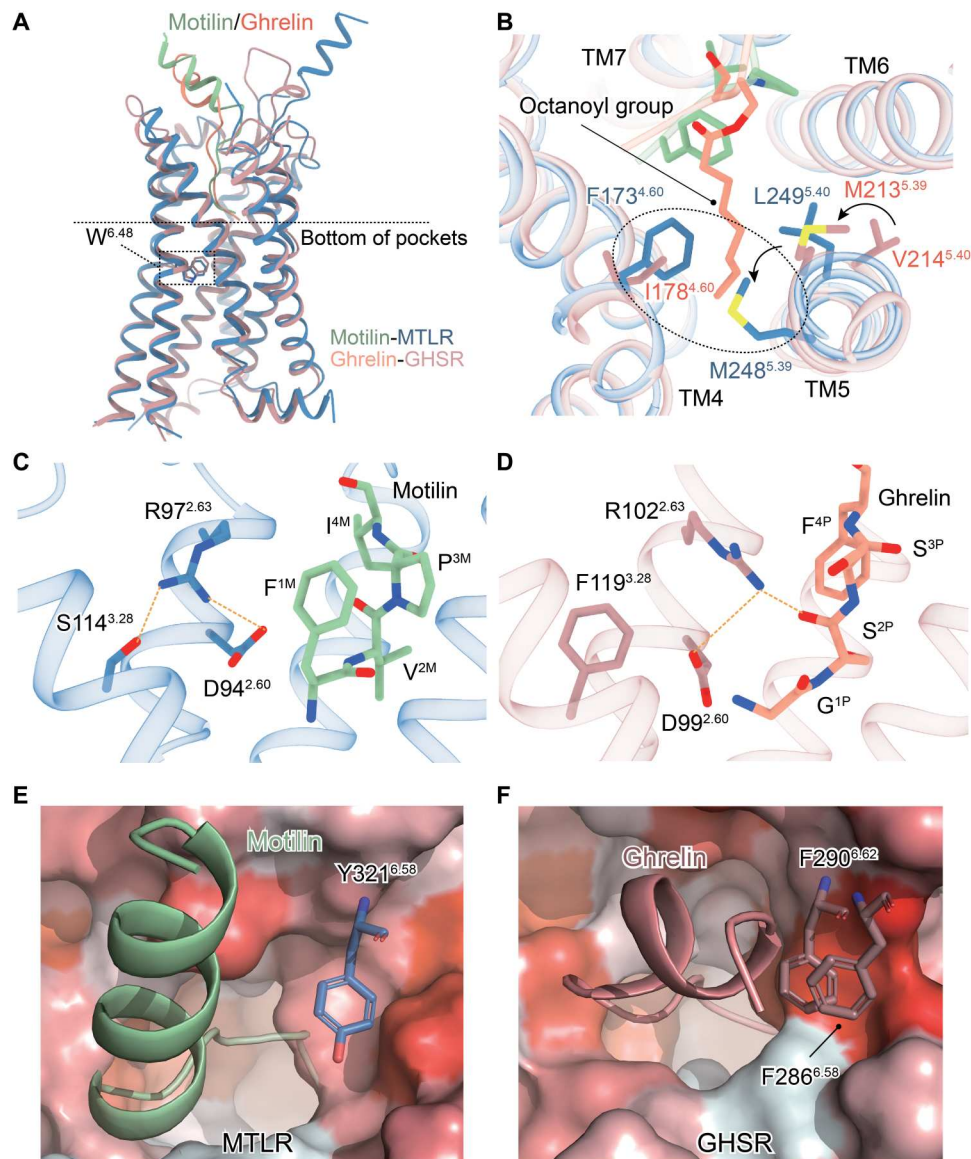
Peptide specificity for MTLR and GHSR

Motilin and ghrelin belong to the ghrelin/motilin-related peptide family, sharing a 36% sequence identity. Their receptors, MTLR and GHSR, also exhibit a remarkable overall sequence similarity (52%), with an 86% identity in their TMDs. Both peptides participate in stimulating GI motility and accelerating gastric emptying. However, they do not show cross-reactivity for MTLR and GHSR (36). A structural comparison of MTLR and GHSR complexes offers a template for explaining the peptide recognition specificity.

The overall structures of MTLR and GHSR are similar, with an RMSD of 0.819 Å, while both peptides apply a similar pose and depth in the binding pocket (Fig. 3A). The high sequence identity of TMD of both receptors produces relatively conserved peptide-binding environments (fig. S7, A to C). However, a structural discrepancy in TM4 and TM5 may determine the peptide selectivity. $F173^{4.60}$ of MTLR may sterically clash with the octanoyl group of
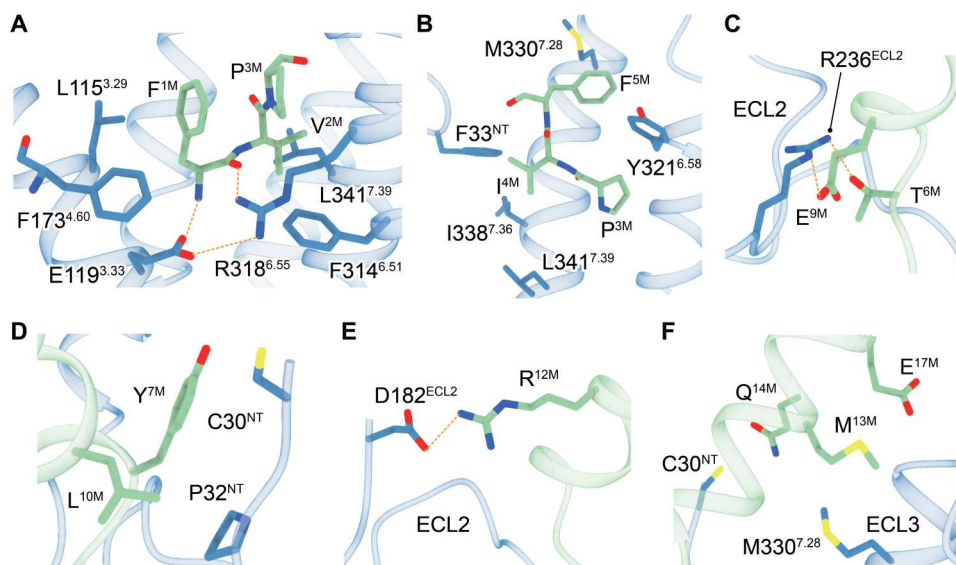
Fig. 2. Recognition of motilin by MTLR. (**A** and **B**) Interaction networks of F^{1M}, V^{2M}, and P^{3M} (A) as well as I^{4M} and F^{5M} (B) in the orthosteric subpocket. (**C** to **F**) Detailed interactions between motilin and residues in the extracellular subpocket of MTLR. The binding site of T^{6M} and E^{9M} (C), Y^{7M} and L^{10M} (D), R^{12M} (E), and M^{13M}, Q^{14M}, and E^{17M} (F). Side chains of residues are displayed in sticks. Hydrogen bonds and salt bridges are depicted as orange dashed lines.

Fig. 3. Peptide specificity for MTLR and GHSR. (**A**) Comparison of the overall structures of active MTLR and GHSR (PDB: 7F9Y). (**B**) The potential clashes between the pocket residues in MTLR and the octanoyl group of ghrelin. (**C** and **D**) Comparison of the "D-R-S/F" motif of MTLR (C) and GHSR (D). (**E** and **F**) The possible peptide entrance of hydrophobic passage of MTLR (E) and GHSR (F). The MTLR and GHSR are shown as a surface presentation by hydrophobicity (hydrophobic surface in red). The hydrophobic residues at the entrance are shown as sticks. The side chains are shown as sticks, and the peptides are depicted in cartoon representation.

ghrelin. Furthermore, the extracellular end of TM5 of MTLR shows an obvious outward rotation relative to GHSR, concomitant to the rotation of M248$^{5.39}$ and L249$^{5.40}$ to occupy the binding site of the octanoyl group, thus preventing the binding of ghrelin (Fig. 3B).In addition, D94$^{2.60}$, R97$^{2.63}$, and S114$^{3.28}$ of MTLR constitute a polar cluster, designated as "D-R-S" motif, which does not interact with motilin. Differently, this D-R-S motif is interrupted in GHSR because of the substitution of serine for phenylalanine at position 3.28. The side chain of R102$^{2.63}$ in GHSR shows a notable rotation toward the ligand-binding pocket core and forms a hydrogen bond with the backbone CO group of S^{2P} in ghrelin. (Fig. 3, C and D). Considering that R102$^{2.63}$ is critical for ghrelin binding to GHSR (*32*), the orientation of the R97$^{2.63}$ side chain in MTLR is

unfavorable for making a stable interaction with ghrelin. These structural differences may explain the low selectivity of ghrelin for MTLR.

Besides the subtle differences in the physicochemical properties of binding pockets, the entry of peptide ligands may affect their selectivity. The structures of GHSR reveal a crevasse enriched with hydrophobic resides between TM6 and TM7, including several phenylalanine residues, of which F286$^{6.58}$ and F290$^{6.62}$ are located at the entrance of the binding pocket (*32, 37*). Correspondingly, F286$^{6.58}$ is replaced by Y321$^{6.58}$ in MTLR. In addition, cognate residues of F290$^{6.62}$ is absent because of a shorter TM6 of MTLR relative to GHSR (Fig. 3, E and F). The resulting weaker hydrophobicity at the entrance of the ligand-binding pocket of MTLR may disrupt

the entry of ghrelin and its low reactivity. The octanoyl moiety of ghrelin is thought to be essential for access to the ligand-binding pocket (*38*) and is also responsible for orienting the N terminus of ghrelin to the bottom of the binding pocket to activate GHSR (*32*). The absence of potent hydrophobic moiety for motilin may disfavor its entering into the octanoyl binding site, thus failing in activating GHSR.

Recognition of erythromycin by MTLR

Erythromycin only occupies the orthosteric binding pocket and makes limited interactions with ECLs of MTLR (Fig. 1H). Previous findings support the notion that both ends but not the middle segment of ECL2 is essential for motilin binding; however, these regions are not critical for erythromycin (*16*, *35*), indicative of different binding modes between erythromycin and motilin.

Erythromycin comprises three structural components: a 14-membered lactone ring and two sugar rings, an amino sugar

(desosamine), and a neutral sugar (cladinose) (Fig. 4A). Both lactone ring and sugar moieties are essential for the macrolide activity (*39*). The lactone ring occupies the upper orthosteric binding subpocket, with two sugars sitting deep in the TMD core (Figs. 1H and 4B). Entire erythromycin largely overlaps with the F^{1M}-F^{5M} segment of motilin and constitutes similar ligand-receptor interactions (Fig. 4B). The cladinose ring overlaps with the side chain of F^{1M} and forms similar hydrophobic interactions with $L115^{3.29}$, $F173^{4.60}$, and $F314^{6.51}$ (Fig. 4, B and C). Its desosamine ring is located in a similar binding site of V^{2M} and P^{3M} and makes an intramolecular π-π stacking with the cladinose ring. In addition, the dimethylamino group of desosamine mimics the backbone of F^{1M} and lies within a salt bridge distance with $E119^{3.33}$ (Fig. 4, B and D). $E119^{3.33}$ stabilizes $R318^{6.55}$ by a salt bridge, and the latter further interacts with cladinose (Fig. 4C). Substitution of $E119^{3.33}$ with aspartic acid, which elongated the ionic distance to the desosamine sugar, or acetylation of the *N*-dimethyl amino in erythromycin
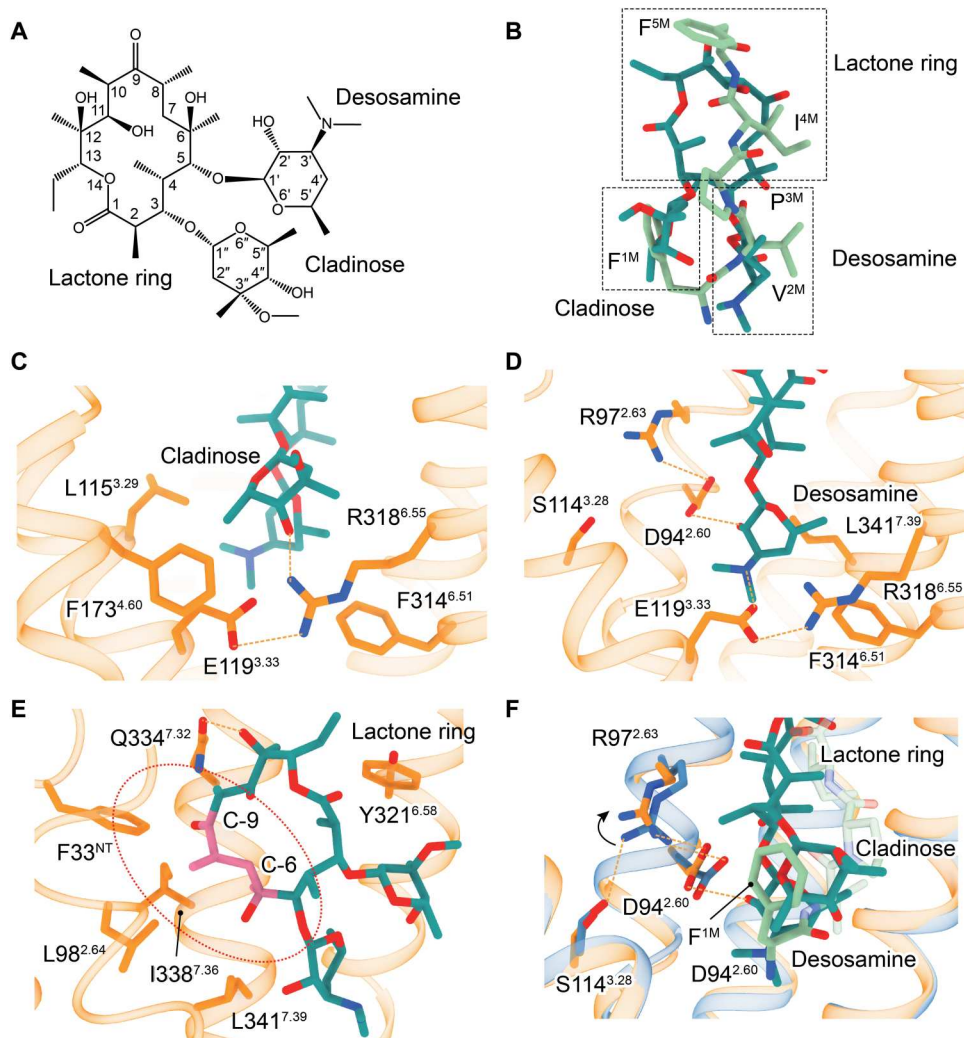
Fig. 4. Recognition of erythromycin by MTLR. (**A**) The chemical structure of erythromycin. Erythromycin can be divided into three components: a lactone ring, an amino sugar (desosamine), and a neutral sugar (cladinose). (**B**) Comparison of the spatial structures of motilin and erythromycin. (**C** to **E**) Detailed interactions between cladinose (C), desosamine (D), the lactone ring (E), and residues in MTLR. (**F**) The different conformation of D-R-S motif in motilin- and erythromycin-bound MTLR structures. The side chains are displayed as sticks. Hydrogen bonds and salt bridges are depicted as orange dashed lines. The shift of the side chain of $R97^{2.63}$ from motilin bound to erythromycin-bound MTLR is indicated by a black arrow.

derivative caused marked decrease in ligand activity, which is assumed to interrupt this ionic interaction (*16*). Besides, the desosamine ring also provides hydrophobic interactions with $F314^{6.51}$ and $L341^{7.39}$ (Fig. 4D). The hydroxyl group on the desosamine ring forms a hydrogen bond with $D94^{2.60}$, which further makes a salt bridge with $R97^{2.63}$ (Fig. 4D). Differently, $R97^{2.63}$ rotates to form a polar cluster with $D94^{2.60}$ and $S114^{3.28}$ in the motilin-bound MTLR structure (Fig. 4F).

The lactone ring of erythromycin resembles P^{3M}-F^{5M} of motilin and engages the binding pocket residues primarily through hydrophobic interactions (Fig. 4E). The number of carbons in the lactone ring is reported to be critical for the macrolide activity, as macrolides with only 12-, 14-, and 15-member but not 16-member lactone rings can activate MTLR (*15*, *39*). In addition, the region from C-6 to C-9 appears to be important for erythromycin activity (*39*), which is in agreement with the markedly decreased erythromycin activities toward MTLR-bearing alanine mutations of residues surrounding this segment, such as $L341^{7.39}$ (fig. S8 and table S3). Besides, 12-hydroxyl forms a hydrogen bond with $Q334^{7.32}$ (Fig. 4E). These findings answer the issue of how a structure-unrelated macrolide binds to MTLR.

Comparison of erythromycin recognition by MTLR and the bacterial ribosome

The erythromycin-bound MTLR complex structure provides a template for comparing its binding modes in MTLR and the ribosome. Erythromycin is embraced by segments of 23*S* ribosomal RNA at the peptidyl transferase cavity and does not directly contact with ribosomal proteins (*40*). Its antibacterial effect is attributed to blocking the tunnel that channels the nascent peptides away from the peptidyl transferase center (*40*). Both lactone ring and two sugar moieties are essential for erythromycin activity in promoting GI motility. Erythromycin analogs lacking either or both sugar moieties are inactive (*39*), which coincides with our receptor mutagenesis analysis that residues surrounding both sugars contribute to the activity of erythromycin (fig. S8). The orientation of the cladinose sugar appears to be important for its gastric prokinetic role (*39*); however, it shows a negligible role in the erythromycin-induced antibacterial effect (*41*, *42*). The different necessity of the cladinose sugar in GI motility regulation and antibacterial effect may stem from its distinct ligand-binding modes. The cladinose sugar sits deep and compactly engages with residues in the ligand-binding pocket of MTLR. Conversely, it points to a low-occupancy cavity and does not make substantial interactions with the 23*S* ribosomal RNA (Fig. 5, A and B). In addition, macrolides with atom numbers of the lactone macrocycle from 14 to 16 show antibacterial effects (*43*). However, macrolides with a 16-membered lactone macrocycle are inactive in promoting GI motility (*39*, *44*).

Desosamine, 3-(dimethylamino)-3,4,6-trideoxyglucose, is critical for the bactericidal activity of erythromycin and its derivatives (*45*). The protonated dimethylamino group on the desosamine moiety participates in polar interaction with the backbone of the ribosome (*40*) and is also ion coordinated with $E119^{3.33}$ of MTLR (Fig. 5, C and D). Displacing one methyl group of the dimethylamino group of erythromycin with an ethyl or isopropyl group markedly increased GI motion–simulating activity but showed no antibacterial activity (*46*). These findings are supported by our structural observation that the dimethylamino group faces the backbone of the ribosome without any extra space to accommodate

bulkier modifications, while a relatively larger space exists surrounding its binding site in MTLR (Fig. 5, E and F). These findings clarify the differences in erythromycin binding modes for MTLR and the ribosome and offer an opportunity for the development of macrolide derivatives with prokinetic activity but devoid of antibacterial activity, termed "motilide."

## Common activation features of the MTLR-related subfamily

MTLR bound to motilin and erythromycin adopts classic active conformations of class A GPCRs. Compared with GHSR bound to an antagonist [Protein Data Bank (PDB): 6KO5], the cytoplasmic end of TM6 of MTLR undergoes a pronounced outward movement, while the cytoplasmic part of TM7 shifts inward (Fig. 6, A to C). Besides GHSR, the sequence of MTLR is most related to neuromedin U receptors, neurotensin receptors, and GPR39 (*47*). Our MTLR structure adds to the pool for understanding the common features of this receptor subfamily.

Endogenous peptides, including motilin, ghrelin, neuromedin U/S, and neurotensin, do not directly reach $W^{6.48}$, the conserved "toggle switch" residue, which often undergoes a conformational change upon ligand binding (*48*). The evolutionarily conserved salt-bridge between $E/D^{3.33}$ and $R^{6.55}$ blocks the further insertion of the peptide ligand and initiates the downward signal transmission. For GHSR and neurotensin receptor 1 (NTSR1) with known structures in the active and inactive states, peptide binding causes an outward rotation of the side chain of the arginine at 6.55 apart from the pocket core and triggers a conformational change of $W^{6.48}$ (Fig. 6, D and E). Specifically, the N-groups of motilin may push $R318^{6.55}$ away from the core to initiate a cascade of conformational alteration (Fig. 6E). Compared with the active GHSR, NTSR1, and neuromedin U receptors (NMURs), the active MTLR shows a nearly merged side-chain conformation of $R^{6.55}$, indicating a conserved receptor activation mechanism across this subfamily (fig. S9).

In addition, several hydrophobic residues, designated as "hydrophobic lock" (*27*, *32*), link the bottom of the binding pocket and conserved "micro-switches" and may participate in the signaltransmission. The hydrophobic residues at positions $F^{6.51}$, $F^{7.42}$, and $Y/F^{7.43}$ in NTSR1, GHSR, and NMUR1 are involved in the agonism transmission (fig. S7D). For MTLR, $F314^{6.51}$, $F344^{7.42}$, and $Y345^{7.43}$ are also associated with motilin-induced MTLR activation (Fig. 6F; fig. S6, E and F; and table S2). The resulting rearrangement of this hydrophobic region causes the conformational changes of micro-switches residues, including toggle switch, ERY, PIF, and NPxxY (Fig. 6, G to I), and lastly leads to the pronounced outward displacement of the cytoplasmic end of TM6 to accommodate the G protein (Fig. 6, A and C).

ICL2-Gα interface of MTLR-related receptors

Members of the MTLR-related GPCR subfamily primarily couple to G_q protein. A previous finding claims the importance of intracellular loop 2 (ICL2) in G_q protein–coupling selectivity (Fig. 7A) (*33*). Because of the invisibility of ICL2 density in the motilin-MTLR-G_q complex, we thus apply the structure of the erythromycin-MTLR-G_q complex to compare the ICL2-Gα interface of MTLR-related receptors. Different from the α-helical conformation of ICL2 in other homolog receptors with known structures, ICL2 of MTLR adopts a loop-like conformation (Fig. 7, B to F). Structural comparison of G_q-coupled MTLR, GHSR (PDB: 7F9Y), NMUR1/2 (PDB: 7W53 and 7W55), and G_i-coupled NTSR1 (PDB: 6OS9) reveals an
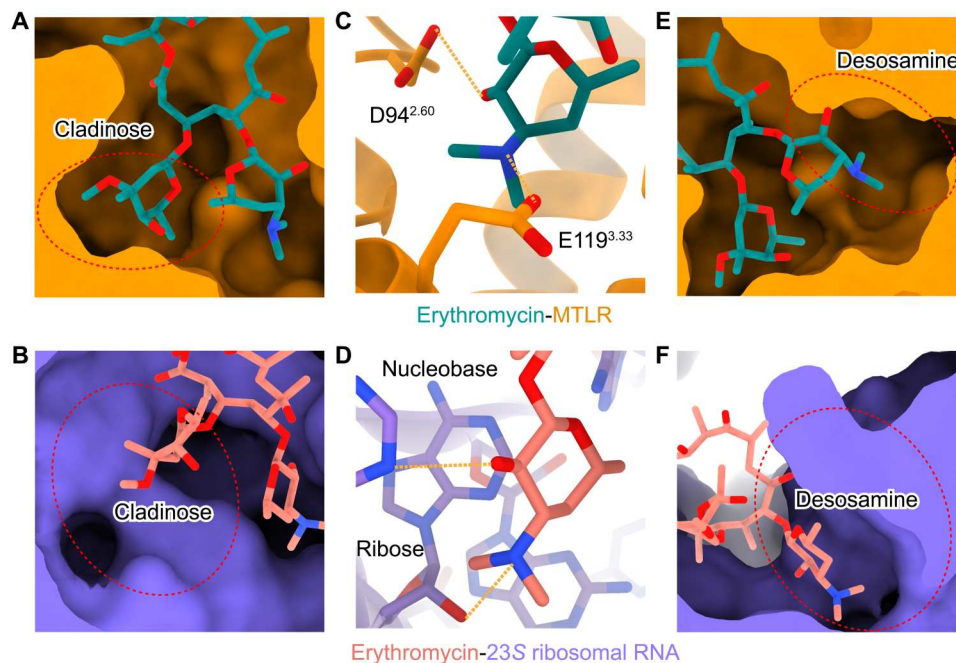
Fig. 5. Comparison of erythromycin recognition by MTLR and the bacterial ribosome. (**A** and **B**) Comparison of the cladinose sugar binding site in MTLR (A) and ribosome (B) (PDB: 1JZY). (**C** and **D**) Interactions between the desosamine sugar and residues in MTLR (C) and ribosome (D). The 2′-OH of erythromycin and the dimethylamino group of desosamine form polar interactions with MTLR and the ribosome. (**E** and **F**) Comparison of the desosamine sugar binding sites in MTLR (E) and the ribosome (F). Polar interactions are displayed by orange dashed lines.

overall conserved interface between ICL2 and the αN and α5 of the Gα subunit. The conserved hydrophobic residue (leucine for MTLR, GHSR, and NMUR1 and phenylalanine for NMUR2 and NTSR1) at position 34.51 packs ICL2 against the hydrophobic pocket in the Gα subunit (Fig. 7, B to F, and fig. S10). It is thought that residues at 34.54 or 34.55 in ICL2 are arginine or lysine in G_q-coupled GPCRs, which interact with residues in αN of the $Gα_q$ subunit and probably are involved in the G_q coupling of GPCRs (33). Consistently, the residue at 34.54 of GHSR forms backbone−side chain polar interactions with R32 of the $Gα_q$ subunit (Fig. 7C). For NMUR1/2, besides residues at 34.54, backbone CO groups of residues at 34.55 are involved in polar interactions with side chains of R31 and R32 (Fig. 7, D and E). Similarly, R147[34.54] of MTLR makes a polar interaction with the $Gα_q$ subunit. This polar interaction may distort the α helix, thus leading to a loop-like ICL2 conformation of MTLR (Fig. 7B). In addition, it is reasonable that a corresponding main chain−sidechain polar interaction also exists between T178[34.55] of NTSR1 and R32 of the $Gα_i$ subunit (Fig. 7F), as NTSR1 primarily couples to G_q protein. These structural observations provide a rationale for understanding the roles of ICL2 in the G_q coupling of MTLR-related receptors.

DISCUSSION

Here, we reported two cryo-EM structures of chimeric G_q-coupled MTLR bound to two structurally unrelated ligands: the endogenous peptide motilin and a macrolide antibiotic erythromycin. Combined with mutagenesis analysis, these structures reveal the recognition mechanism of two ligands by MTLR. The extreme N-terminal pentapeptide of motilin buries deeply into the hydrophobic orthosteric subpocket and contributes substantially to peptide activity, while its C-terminal amino acids form an α helix, which engages the extracellular subpocket and is thought to mediate receptor desensitization (20). MTLR owns the second-longest ECL2 (65 amino acids) after the C3a receptor in class A GPCRs. Its ECL2 adopts a unique upright α-helical conformation, which may function as an umbrella shaft to support the large loop region, diversifying the ECL2 conformation of class A GPCRs. However, the lack of density from a majority of ECL2 in our structural model disables us from characterizing its critical roles in motilin binding. In addition, compared with GHSR, the relatively weaker hydrophobicity at the entrance of the ligand-binding pocket of MTLR is unfavorable for ghrelin entry. Besides, steric hindrance caused by cognate residues of the octanoyl group binding site in MTLR probably excludes ghrelin binding, which may explain the nonreactivity of MTLR for ghrelin. The lower hydrophobicity of motilin relative to acylated ghrelin disfavors its entering into the GHSR binding pocket, which may contribute to its low selectivity for GHSR. In addition, to our knowledge, MTLR was the first reported GPCR being activated by antibiotics (11, 14, 17). Erythromycin, the first identified macrolide antibiotic for clinical use (49), only occupies the orthosteric subpocket and ensembles the N-terminal pentapeptide of motilin. Structure comparison of erythromycin bound to MTLR and ribosome reveals different erythromycin binding modes and offers an opportunity for the development of motilide, i.e., macrolide derivatives with prokinetic activity but devoid of antibacterial activity.

Three types of MTLR agonists have progressed to clinical evaluation, including peptide analogs, motilides, and nonmacrolide small molecular compounds. Peptide analogs include KW-5139 ([Leu[13]]-
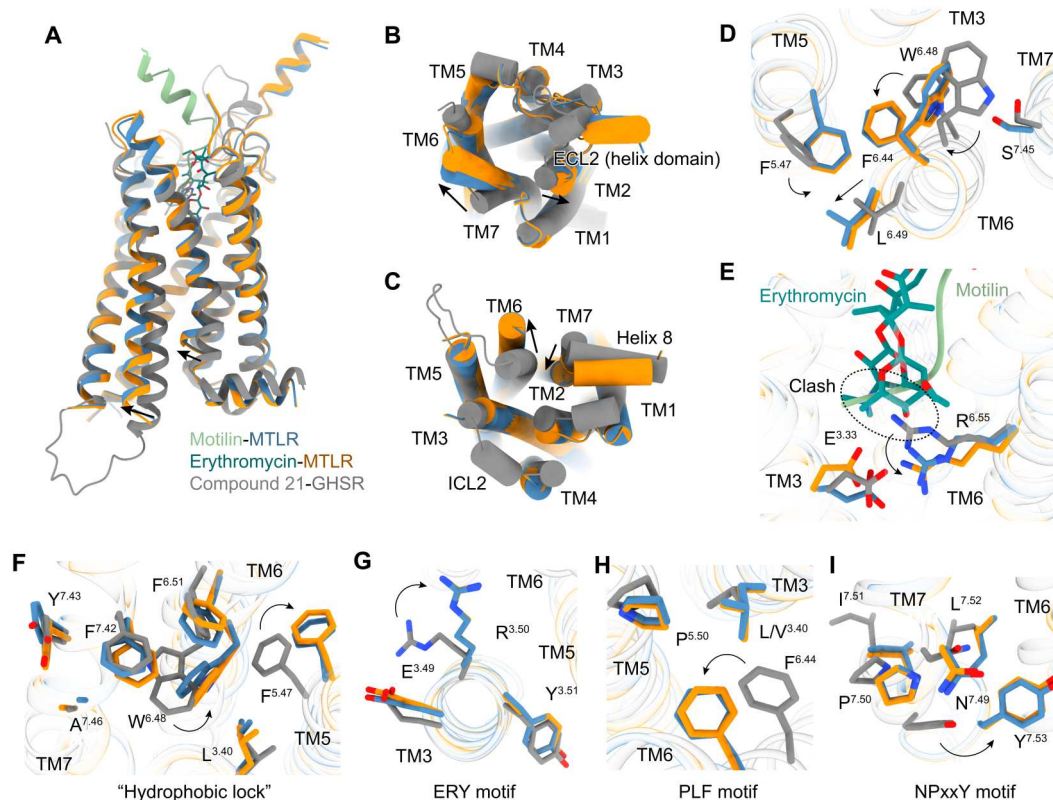
Fig. 6. Activation mechanism of MTLR. (**A**) Structural superposition of active MTLRs and the inactive GHSR (PDB: 6KO5) from the side view. The movement directions of TMs of MTLR relative to that of GHSR are highlighted as black arrows. (**B** and **C**) The extracellular (B) and intracellular (C) views of active MTLRs and the inactive GHSR. (**D**) Conformational changes of $W^{6.48}$. (**E**) The rotation of the conserved salt bridge upon MTLR activation. (**F** to **I**) Conformational changes of the micro-switches upon receptor activation, including the hydrophobic lock (F), ERY (G), PLF (H), and NPxxY motifs (I). The rotation directions of residue side chains upon MTLR activation compared with the antagonist-bound GHSR are indicated by black arrows.

motilin) and atilmotin (*21*), of which the latter shows improved receptor selectivity and is not associated with any central nervous system−, respiratory system−, or cardiovascular system−related adverse effects (*50*). The macrolide antibiotic erythromycin and azithromycin have been shown to mimic the GI motility activity of motilin (*9, 51*). Although the doses are lower than that used for antibacterial use, concerns over safety and potential exacerbation of antibiotic resistance are still raised. Several motilides, such as ABT-229 and mitemcinal (GM-611), with higher specificity for MTLR and devoid of antibacterial activity, were further developed. However, ABT-229 shows a more potent desensitization-inducing effect compared with motilin and erythromycin due to its relatively high ability to induce receptor internalization (*52, 53*). The desensitization effect of mitemcinal is much more improved (*54*). Non-macrolide small molecular agonists, such as camicinal (GSK-962040), RQ-00201894, and DS-3801b, were designed to improve pharmacokinetics properties and minimize self-desensitization (*24–26*). Camicinal is an orally effective MTLR agonist with high receptor selectivity, which shows long-lasting gastric cholinergic activity (*51*). Although extensive efforts have been made to develop MTLR-targeting drug candidates, all these candidates are discontinued in clinical trials because of undesirable safety and effectiveness. The accurate structural information on ligand recognition provides the basis for designing drugs targeting MTLR and offers an opportunity for the treatment of GI motility disorder.

MATERIALS AND METHODS
Constructs
The full-length human MTLR was modified to contain the N-terminal thermally stabilized BRIL to enhance receptor expression, followed by an N-terminal Flag tag, a 10× His-tag, and a tobacco etch virus (TEV) cleavage site. LgBiT was also inserted at the C terminus of the human MTLR with a linker (GSSGGGGSGGGGSSG) using homologous recombination. The modified MTLR was cloned into the pFastBac vectors (Thermo Fisher Scientific) using the ClonExpress II One Step Cloning Kit (Vazyme Biotech). An engineered $G\alpha_q$ chimera was generated on the basis of the mini-$G\alpha_s$ scaffold with its N terminus replaced by corresponding sequences of $G\alpha_{i1}$, designated as $mG\alpha_{s/q/iN}$. Human WT $G\beta1$, human $G\gamma2$, and a single-chain antibody scFv16, as well as a $G\beta1$ fused with SmBiT at its C terminus, were cloned into pFastBac vectors.

Insect cell expression
Human MTLR, G_q chimera, $G\beta_1$, $G\gamma$, scFv16, and Ric8a were coexpressed in High Five insect cells (Invitrogen) using the baculovirus method (Expression Systems). Cell cultures were grown in ESF 921 serum-free medium (Expression Systems) to a density of 2 million to 3 million cells/ml and then infected with six separate baculoviruses at a suitable ratio. The culture was collected by centrifugation 48 hours after infection, and cell pellets were stored at −80°C.
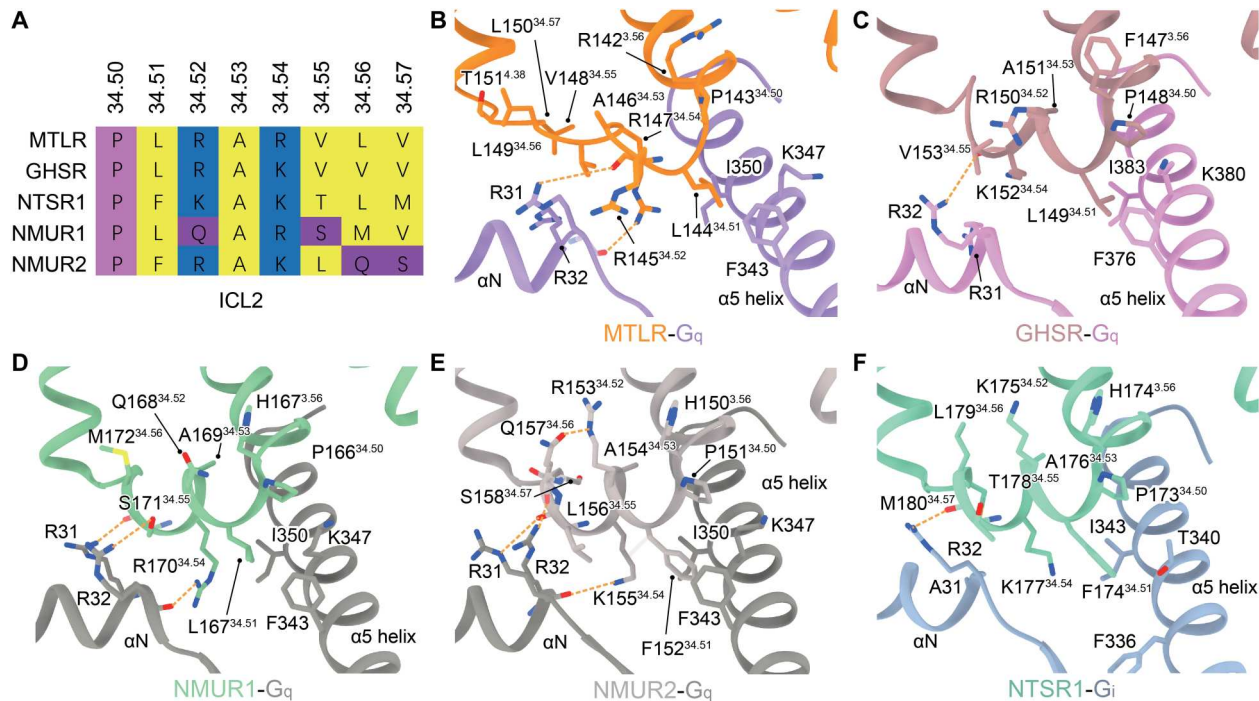
Fig. 7. ICL2-Gα interface of MTLR-related receptors. (A) Sequence comparison of ICL2 of MTLR, GHSR, NTSR1, NMUR1, and NMUR2. (**B** to **F**) Interfaces between the Gα subunit and ICL2 of MTLR-G_q (B), GHSR-G_q (PDB: 7F9Y) (C), NMUR1-G_q (PDB: 7W53) (D), NMUR2-G_q (PDB: 7W55) (E), and NTSR1-G_i (PDB: 6OS9) (F). The colors are shown as indicated. Polar interactions are indicated by orange dashed lines.

Complex purification

Cell pellets were thawed in 20 mM Hepes (pH 7.4), 50 mM NaCl, 10 mM $MgCl_2$, and $CaCl_2$ supplemented with Protease Inhibitor Cocktail (TargetMol). For the motilin-MTLR-G_q-scFv16 complex, 15 µM motilin (GenScript) and apyrase (25 mU ml^{-1}; Sigma-Aldrich) were added. For the erythromycin-MTLR-G_q-scFv16 complex, 1 mM erythromycin (Sangon Biotech) and apyrase (25 mU ml^{-1}; Sigma-Aldrich) were added. The suspension was incubated for 1 hour at room temperature, and the complex was solubilized from the membrane using 0.5% (w/v) lauryl maltose neopentyl glycol (LMNG; Anatrace) and 0.1% (w/v) cholesteryl hemisuccinate (CHS; Anatrace) for 2 hours at 4°C. Insoluble material was removed by centrifugation at 65,000g for 35 min, and the supernatant was purified by nickel affinity chromatography (Ni Smart Beads 6FF, SMART Lifesciences). The resin was then packed and washed with 20 column volumes of 20 mM Hepes (pH 7.4), 50 mM NaCl, 0.01% (w/v) LMNG, and 0.002% CHS. The complex sample was eluted in a buffer containing 300 mM imidazole and concentrated using an Amicon Ultra Centrifugal Filter (molecular weight cut-off, 100 kDa). The complex was then subjected to size exclusion chromatography on a Superdex 200 Increase 10/300 column (GE Healthcare) preequilibrated with size buffer containing 20 mM Hepes (pH 7.4), 100 mM NaCl, 0.00075% (w/v) LMNG, 0.00025% (w/v) glyco-diosgenin (GDN) (Anatrace), and 0.00015% CHS to separate complexes. For the MTLR complexes, 15 µM motilin and 1 mM erythromycin were included in the size buffer. Eluted fractions were evaluated by SDS–polyacrylamide gel electrophoresis, and those consisting of receptor-G_q protein complex were pooled and concentrated for cryo-EM experiments.

Cryo-EM data collection

Cryo-EM grids were prepared with the Vitrobot Mark IV plunger (Thermo Fisher Scientific) set to 4°C and 100% humidity. Three microliters of the erythromycin-MTLR complex were applied to the glow-discharged copper R1.2/1.3 holey carbon grids. The sample was incubated for 20 s on the grids before blotting for 3 s (double-sided, blot force −1) and flash-frozen in liquid ethane immediately. The same condition was used for the sample motilin-MTLR complex.

For the erythromycin-MTLR-G_q-scFv16 complex dataset, 3230 movies were collected on a Titan Krios equipped with a Gatan K3 direct electron detection device at 300 kV with a magnification of 81,000, corresponding to a pixel size 1.07 Å. Image acquisition was performed with EPU Software (Thermo Fisher Scientific, Eindhoven, Netherlands). We collected a total of 36 frames accumulating to a total dose of 50 e^- $Å^{-2}$ over 2.5-s exposure on each TIF format movie.

For the motilin-MTLR-G_q-scFv16 complex, five datasets including 31,157 movies were collected on a Titan Krios equipped with a Gatan K3 direct electron detection device at 300 kV with a magnification of 105,000, corresponding to a pixel size 0.824 Å. Image acquisition was performed with EPU Software (Thermo Fisher Scientific, Eindhoven, the Netherlands). We collected a total of 36 frames accumulating to a total dose of 50 e^- $Å^{-2}$ over 2.5 s exposure on each TIFF format movie. A larger number of movies are applied to overcome the preferred orientations of the motilin-bound MTLR complex compared with the erythromycin-bound one.

Cryo-EM image processing

MotionCor2.1 was used to perform the frame-based motion-correction algorithm to generate drift-corrected micrographs for further processing and CTFFIND4.1 provided the estimation of the contrast transfer function (CTF) parameters (55, 56). For the erythromycin-MTLR-G_q-scFv16 complex dataset, 63 aligned micrographs were deleted because of contaminations or bad ice quality. After selection, approximately 1000 particles were manually picked, and two-dimensional (2D) classes were calculated and used as references for automatic picking. All subsequent steps of particle picking, extraction, classification, and postprocessing of refined models were performed with Relion4.0 (57). A total of 2,906,240 particles were extracted from the cryo-EM micrographs and followed by three rounds of reference-free 2D classification, yielding 2,471,438 particles after clearance. Six rounds of 3D classification were used to separate 261,108 particles that resulted in a clearer density of the whole complex. We refined this portion of particles, which led to a structure at 3.97-Å global resolution. After contrast transfer function (CTF) refinement, Bayesian polishing, and postprocessing, DeepEMhancer, a deep-learning approach for automatic postprocessing of cryo-EM maps, was also applied to reduce noise levels and obtain more details of the experimental maps (58). The particles were lastly reconstituted to a 3.51-Å structure.

For the motilin-MTLR-G_q-scFv16 complex, each dataset was processed separately with autopicking and 2D classification. On the basis of the MTLR density, a mask was generated using RELION and was used in the mask 3D classification on the receptor part, which could separate particles that resulted in a clearer density of MTLR. After selection, all portions from five different datasets were pooled together, which was followed by one more global 3D classification. We refined the remaining 1,174,882 particles, which were reconstituted to a 3.52-Å structure. After the postprocessing, the structure reached 3.19-Å global resolution. The final density map was also processed with DeepEMhancer.

Model building

MTLR structure predicted from AlphaFold 2 was used as the starting reference model for receptor building (34). Structures of $G\alpha_q$, Gβ, Gγ, and scFv16 derived from PDB entry 7WKD were rigid body fit into the density. All models were fitted into the EM density map using UCSF Chimera followed by iterative rounds of manual adjustment and automated rebuilding in COOT and PHENIX, respectively. The model was finalized by rebuilding in ISOLDE (59), followed by refinement in PHENIX with torsion-angle restraints to the input model. The final model statistics were validated using comprehensive validation (cryo-EM) in PHENIX (60) and provided in table S1. All structural figures were prepared using Chimera, Chimera X, and PyMOL (Schrödinger LLC.).

Inositol phosphate accumulation assay

The inositol phosphate IP1 accumulation assay was applied to evaluate the G_q signals of MTLR. IP1 production was measured using the IP-One HTRF kit (Cisbio). Briefly, AD-293 cells (Agilent) were grown to a density of 400,000 to 500,000 cells/ml and then infected with separate plasmids at a suitable concentration. The culture was collected by centrifugation 24 hours after incubation at 37°C in 5% CO_2 with a stimulation buffer. The cell suspension was then dispensed in a white 384-well plate at a volume of 7 μl per well before adding 7 μl of ligands. The mixture was incubated for 1 hour at 37°C. IP1-d2 and anti-IP1 cryptate dissolved in lysis buffer (3 μl each) were subsequently added and incubated for 15 to 30 min at room temperature before measurement. Intracellular IP1 measurement was carried out with the IP-One HTRF kit and EnVision multi-plate reader (PerkinElmer) according to the manufacturer's instructions. Data were normalized to the baseline response of the ligand.

Measurement of cell surface expression

Cell surface expression of MTLR (WT) and mutants was performed using AD-293 cells (Agilent) cultured in Dulbecco's Modified Eagle's Medium containing 10% (v/v) fetal bovine serum at 37°C in 5% CO_2. Cells grown to a density of 200,000 to 250,000 cells/ml were transiently transfected with WT or mutant plasmids of MTLR for 24 hours. The transfected cells were collected and blocked with 5% (w/v) bovine serum albumin (BSA) in phosphate-buffered saline (PBS) for 15 min at room temperature before incubating with primary anti-Flag antibody (diluted with PBS containing 5% BSA at a ratio of 1:150; ABclonal) for 1 hour at room temperature. Cells were washed three times with PBS containing 1% (w/v) BSA and then incubated with anti-mouse Alexa Fluor 488–conjugated secondary antibody diluting at a ratio of 1:1000 (Invitrogen) for 2 hours at 4°C in the dark. After another three washes, cells were suspended in 200 μl of PBS containing 1% BSA. The surface expression of the MTLR was monitored by detecting the fluorescent intensity of Alexa Fluor 488 using a BD Accuri C6 (excitation, 488 nm and emission, 519 nm). Data were analyzed by BD Accuri C6 software 1.0.264.

Quantification and statistical analysis

All functional study data were analyzed using GraphPad Prism 8.0 (GraphPad Software Inc.) and showed as means ± SEM from at least three independent experiments in triplicate. Concentration-response curves were evaluated with a three-parameter logistic equation. The significance was determined with the one-way analysis of variance test with Tukey's test. *$P < 0.05$ was considered statistically significant.

Supplementary Materials

This PDF file includes:
Figs. S1 to S10
Tables S1 to S3

REFERENCES AND NOTES

1. J. C. Brown, V. Mutt, J. R. Dryburgh, The further purification of motilin, a gastric motor activity stimulating polypeptide from the mucosa of the small intestine of hogs. *Can. J. Physiol. Pharmacol.* **49**, 399–405 (1971).
2. G. J. Sanger, J. B. Furness, Ghrelin and motilin receptors as drug targets for gastrointestinal disorders. *Nat. Rev. Gastroenterol. Hepatol.* **13**, 38–48 (2016).
3. T. Kitazawa, H. Kaiya, Motilin comparative study: Structure, distribution, receptors, and gastrointestinal motility. *Front. Endocrinol.* **12**, 700884 (2021).
4. S. D. Feighner, C. P. Tan, K. K. McKee, O. C. Palyha, D. L. Hreniuk, S. S. Pong, C. P. Austin, D. Figueroa, D. MacNeil, M. A. Cascieri, R. Nargund, R. Bakshi, M. Abramovitz, R. Stocco, S. Kargman, G. O'Neill, L. H. T. van der, Ploeg, J. Evans, A. A. Patchett, R. G. Smith, A. D. Howard, Receptor for motilin identified in the human gastrointestinal system. *Science* **284**, 2184–2188 (1999).

5. J. He, D. M. Irwin, R. Chen, Y. P. Zhang, Stepwise loss of motilin and its specific receptor genes in rodents. *J. Mol. Endocrinol.* **44**, 37–44 (2010).

6. J. T. Andersen, M. B. Daba, G. Berntzen, T. E. Michaelsen, I. Sandlie, Cross-species binding analyses of mouse and human neonatal Fc receptor show dramatic differences in immunoglobulin G and albumin binding. *J. Biol. Chem.* **285**, 4826–4836 (2010).

7. G. J. Sanger, Why is motilin active in some studies with mice, rats, and guinea pigs, but not in others? Implications for functional variability among rodents. *Pharmacol. Res. Perspect.* **10**, e00900 (2022).

8. E. Deloose, W. Verbeure, I. Depoortere, J. Tack, Motilin: From gastric motility stimulation to hunger signalling. *Nat. Rev. Endocrinol.* **15**, 238–250 (2019).

9. Z. Itoh, M. Nakaya, T. Suzuki, H. Arai, K. Wakabayashi, Erythromycin mimics exogenous motilin in gastrointestinal contractile activity in the dog. *Am. J. Physiol.* **247**, G688–G694 (1984).

10. Y. Kondo, K. Torii, Z. Itoh, S. Omura, Erythromycin and its derivatives with motilin-like biological activities inhibit the specific binding of 125I-motilin to duodenal muscle. *Biochem. Biophys. Res. Commun.* **150**, 877–882 (1988).

11. T. Peeters, G. Matthijs, I. Depoortere, T. Cachet, J. Hoogmartens, G. Vantrappen, Erythromycin is a motilin receptor agonist. *Am. J. Physiol.* **257**, G470–G474 (1989).

12. R. W. Finberg, R. C. Moellering, F. P. Tally, W. A. Craig, G. A. Pankey, E. P. Dellinger, M. A. West, M. Joshi, P. K. Linden, K. V. Rolston, J. C. Rotschafer, M. J. Rybak, The importance of bactericidal drugs: Future directions in infectious disease. *Clin. Infect. Dis.* **39**, 1314–1320 (2004).

13. M. Morar, K. Pengelly, K. Koteva, G. D. Wright, Mechanism and diversity of the erythromycin esterase family of enzymes. *Biochemistry* **51**, 1740–1751 (2012).

14. D. Zhao, A. C. Meyer-Gerspach, E. Deloose, J. Iven, N. Weltens, I. Depoortere, O. O'daly, J. Tack, L. van Oudenhove, The motilin agonist erythromycin increases hunger by modulating homeostatic and hedonic brain circuits in healthy women: A randomized, placebo-controlled study. *Sci. Rep.* **8**, 1819 (2018).

15. J. Broad, G. J. Sanger, The antibiotic azithromycin is a motilin receptor agonist in human stomach: Comparison with erythromycin. *Br. J. Pharmacol.* **168**, 1859–1867 (2013).

16. L. Xu, I. Depoortere, P. Vertongen, P. Waelbroeck, P. Robberecht, T. L. Peeters, Motilin and erythromycin-A share a common binding site in the third transmembrane segment of the motilin receptor. *Biochem. Pharmacol.* **70**, 879–887 (2005).

17. F. H. Weber Jr., R. D. Richards, R. W. McCallum, Erythromycin: A motilin agonist and gastrointestinal prokinetic agent. *Am. J. Gastroenterol.* **88**, 485–490 (1993).

18. V. Annese, G. Lombardi, V. Frusciante, U. Germani, A. Andriulli, G. Bassotti, Cisapride and erythromycin prokinetic effects in gastroparesis due to type 1 (insulin-dependent) diabetes mellitus. *Aliment. Pharmacol. Ther.* **11**, 599–603 (1997).

19. E. M. Jarvie, V. J. North Laidler, S. Corcoran, A. Bassil, G. J. Sanger, Differences between the abilities of tegaserod and motilin receptor agonists to stimulate gastric motility in vitro. *Br. J. Pharmacol.* **150**, 455–462 (2007).

20. A. Mitselos, I. Depoortere, T. L. Peeters, Delineation of the motilin domain involved in desensitization and internalization of the motilin receptor by using full and partial antagonists. *Biochem. Pharmacol.* **73**, 115–124 (2007).

21. A. Korimilli, H. P. Parkman, Effect of atilmotin, a motilin receptor agonist, on esophageal, lower esophageal sphincter, and gastric pressures. *Dig. Dis. Sci.* **55**, 300–306 (2010).

22. Z. Itoh, Motilin and clinical application. *Peptides* **18**, 593–608 (1997).

23. G. J. Sanger, Y. Wang, A. Hobson, J. Broad, Motilin: Towards a new understanding of the gastrointestinal neuropharmacology and therapeutic use of motilin receptor agonists. *Br. J. Pharmacol.* **170**, 1323–1332 (2013).

24. J. Broad, N. Takahashi, M. Tajimi, M. Sudo, A. Góralczyk, U. Parampalli, K. Mannur, T. Yamamoto, G. J. Sanger, RQ-00201894: A motilin receptor agonist causing long-lasting facilitation of human gastric cholinergically-mediated contractions. *J. Pharmacol. Sci.* **130**, 60–65 (2016).

25. N. Toda, T. Shida, R. Takano, T. Katagiri, M. Hirouchi, M. Abe, K. Soma, Y. Nakagami, M. Yamazaki, Discovery of DS-3801b, a non-macrolide GPR38 agonist with N-methylanilide structure. *Bioorg. Med. Chem. Lett.* **59**, 128554 (2022).

26. G. J. Sanger, S. M. Westaway, A. A. Barnes, D. T. Macpherson, A. I. Muir, E. M. Jarvie, V. N. Bolton, S. Cellek, E. Näslund, P. M. Hellström, R. A. Borman, W. P. Unsworth, K. L. Matthews, K. Lee, GSK962040: A small molecule, selective motilin receptor agonist, effective as a stimulant of human and rabbit gastrointestinal motility. *Neurogastroenterol. Motil.* **21**, 657–664 (2009).

27. C. You, Y. Zhang, P. Xu, S. Huang, W. Yin, H. Eric Xu, Y. Jiang, Structural insights into the peptide selectivity and activation of human neuromedin U receptors. *Nat. Commun.* **13**, 2045 (2022).

28. J. Duan, D.-d. Shen, X. E. Zhou, P. Bi, Q.-f. Liu, Y.-x. Tan, Y.-w. Zhuang, H.-b. Zhang, P.-y. Xu, S.-j. Huang, S.-s. Ma, X.-h. He, K. Melcher, Y. Zhang, H. E. Xu, Y. Jiang, Cryo-EM structure of an activated VIP1 receptor-G protein complex revealed by a NanoBiT tethering strategy. *Nat. Commun.* **11**, 4121 (2020).

29. R. Nehmé, B. Carpenter, A. Singhal, A. Strege, P. C. Edwards, C. F. White, H. du, R. Grisshammer, C. G. Tate, Mini-G proteins: Novel tools for studying GPCRs in their active conformation. *PLOS ONE* **12**, e0175642 (2017).

30. S. Maeda, A. Koehl, H. Matile, H. Hu, D. Hilger, G. F. X. Schertler, A. Manglik, G. Skiniotis, R. J. P. Dawson, B. K. Kobilka, Development of an antibody fragment that stabilizes GPCR/G-protein complexes. *Nat. Commun.* **9**, 3712 (2018).

31. Y. L. Yin, C. Ye, F. Zhou, J. Wang, D. Yang, W. Yin, M. W. Wang, H. E. Xu, Y. Jiang, Molecular basis for kinin selectivity and activation of the human bradykinin receptors. *Nat. Struct. Mol. Biol.* **28**, 755–761 (2021).

32. Y. Wang, S. Guo, Y. Zhuang, Y. Yun, P. Xu, X. He, J. Guo, W. Yin, H. E. Xu, X. Xie, Y. Jiang, Molecular recognition of an acyl-peptide hormone and activation of ghrelin receptor. *Nat. Commun.* **12**, 5064 (2021).

33. J. Duan, D. D. Shen, T. Zhao, S. Guo, X. He, W. Yin, P. Xu, Y. Ji, L. N. Chen, J. Liu, H. Zhang, Q. Liu, Y. Shi, X. Cheng, H. Jiang, H. Eric Xu, Y. Zhang, X. Xie, Y. Jiang, Molecular basis for allosteric agonism and G protein subtype selectivity of galanin receptors. *Nat. Commun.* **13**, 1364 (2022).

34. J. Jumper, R. Evans, A. Pritzel, T. Green, M. Figurnov, O. Ronneberger, K. Tunyasuvunakool, R. Bates, A. Žídek, A. Potapenko, A. Bridgland, C. Meyer, S. A. A. Kohl, A. J. Ballard, A. Cowie, B. Romera-Paredes, S. Nikolov, R. Jain, J. Adler, T. Back, S. Petersen, D. Reiman, E. Clancy, M. Zielinski, M. Steinegger, M. Pacholska, T. Berghammer, S. Bodenstein, D. Silver, O. Vinyals, A. W. Senior, K. Kavukcuoglu, P. Kohli, D. Hassabis, Highly accurate protein structure prediction with AlphaFold. *Nature* **596**, 583–589 (2021).

35. B. Matsuura, M. Dong, L. J. Miller, Differential determinants for peptide and non-peptidyl ligand binding to the motilin receptor. Critical role of second extracellular loop for peptide binding and action. *J Biol Chem* **277**, 9834–9839 (2002).

36. H. Nunoi, B. Matsuura, S. Utsunomiya, T. Ueda, T. Miyake, S. Furukawa, T. Kumagi, Y. Ikeda, M. Abe, Y. Hiasa, M. Onji, A relationship between motilin and growth hormone secretagogue receptors. *Regul. Pept.* **176**, 28–35 (2012).

37. Y. Shiimura, S. Horita, A. Hamamoto, K. Asada, K. Hirata, M. Tanaka, K. Mori, T. Uemura, T. Kobayashi, S. Iwata, M. Kojima, Structure of an antagonist-bound ghrelin receptor reveals possible ghrelin recognition mode. *Nat. Commun.* **11**, 4160 (2020).

38. G. Ferre, M. Louet, O. Saurel, B. Delort, G. Czaplicki, C. M'Kadmi, M. Damian, P. Renault, S. Cantel, L. Gavara, P. Demange, J. Marie, J.-A. Fehrentz, N. Floquet, A. Milon, J.-L. Baneres, Structure and dynamics of G protein-coupled receptor-bound ghrelin reveal the critical role of the octanoyl chain. *Proc. Natl. Acad. Sci. U.S.A.* **116**, 17525–17530 (2019).

39. I. Depoortere, T. L. Peeters, G. Matthijs, T. Cachet, J. Hoogmartens, G. Vantrappen, Structure-activity relation of erythromycin-related macrolides in inducing contractions and in displacing bound motilin in rabbit duodenum. *Neurogastroenterol. Motil.* **1**, 150–159 (1989).

40. F. Schlunzen, R. Zarivach, J. Harms, A. Bashan, A. Tocilj, R. Albrecht, A. Yonath, F. Franceschi, Structural basis for the interaction of antibiotics with the peptidyl transferase centre in eubacteria. *Nature* **413**, 814–821 (2001).

41. S. Nelson, W. R. Summer, P. B. Terry, G. A. Warr, G. J. Jakab, Erythromycin-induced suppression of pulmonary antibacterial defenses: A potential mechanism of superinfection in the lung. *Am. Rev. Respir. Dis.* **136**, 1207–1212 (1987).

42. T. H. Haight, M. Finland, The antibacterial action of erythromycin. *Proc. Soc. Exp. Biol. Med.* **81**, 175–183 (1952).

43. O. Mahama, C. Songuigama, Pharmacochemical aspects of the evolution from erythromycin to neomacrolides, ketolides and neoketolides. *Open J. Med. Chem.* **10**, 57–112 (2020).

44. Z. Itoh, T. Suzuki, M. Nakaya, M. Inoue, H. Arai, K. Wakabayashi, Structure-activity relation among macrolide antibiotics in initiation of interdigestive migrating contractions in the canine gastrointestinal tract. *Am. J. Physiol.* **248**, G320–G325 (1985).

45. A. Nedal, S. B. Zotchev, Biosynthesis of deoxyaminosugars in antibiotic-producing bacteria. *Appl. Microbiol. Biotechnol.* **64**, 7–15 (2004).

46. K. Tsuzuki, T. Sunazuka, S. Marui, H. Toyoda, S. Omura, N. Inatomi, Z. Itoh, Motilides, macrolides with gastrointestinal motor stimulating activity. I. O-substituted and tertiary N-substituted derivatives of 8,9-anhydroerythromycin A 6,9-hemiacetal. *Chem. Pharm. Bull.* **37**, 2687–2700 (1989).

47. K. K. McKee, C. P. Tan, O. C. Palyha, J. Liu, S. D. Feighner, D. L. Hreniuk, R. G. Smith, A. D. Howard, L. H. T. van der Ploeg, Cloning and characterization of two human G protein-coupled receptor genes (GPR38 and GPR39) related to the growth hormone secretagogue and neurotensin receptors. *Genomics* **46**, 426–434 (1997).

48. W. I. Weis, B. K. Kobilka, The molecular basis of G protein-coupled receptor activation. *Annu. Rev. Biochem.* **87**, 897–919 (2018).

49. G. J. McGuire, R. L. Bunch, R. C. Anderson, H. E. Boaz, E. H. Flynn, H. M. Powell, J. W. Smith, llotycin, a new antibiotic. *Antibiot. Chemother.* **2**, 281–283 (1952).

50. M.-I. Park, I. Ferber, M. Camilleri, K. Allenby, R. Trillo, D. Burton, A. R. Zinsmeister, Effect of atilmotin on gastrointestinal transit in healthy subjects: A randomized, placebo-controlled study. *Neurogastroenterol. Motil.* **18**, 28–36 (2006).

51. J. Broad, S. Mukherjee, M. Samadi, J. E. Martin, G. E. Dukes, G. J. Sanger, Regional- and agonist-dependent facilitation of human neurogastrointestinal functions by motilin receptor agonists. *Br. J. Pharmacol.* **167**, 763–774 (2012).

52. V. Lamian, A. Rich, Z. Ma, J. Li, R. Seethala, D. Gordon, Y. Dubaquie, Characterization of agonist-induced motilin receptor trafficking and its implications for tachyphylaxis. *Mol. Pharmacol.* **69**, 109–118 (2006).

53. A. Mitselos, P. Vanden Berghe, T. L. Peeters, I. Depoortere, Differences in motilin receptor desensitization after stimulation with motilin or motilides are due to alternative receptor trafficking. *Biochem. Pharmacol.* **75**, 1115–1128 (2008).

54. H. Takanashi, O. Cynshi, Motilides: A long and winding road: Lessons from mitemcinal (GM-611) on diabetic gastroparesis. *Regul. Pept.* **155**, 18–23 (2009).

55. S. Q. Zheng, E. Palovcak, J. P. Armache, K. A. Verba, Y. Cheng, D. A. Agard, MotionCor2: Anisotropic correction of beam-induced motion for improved cryo-electron microscopy. *Nat. Methods* **14**, 331–332 (2017).

56. A. Rohou, N. Grigorieff, CTFFIND4: Fast and accurate defocus estimation from electron micrographs. *J. Struct. Biol.* **192**, 216–221 (2015).

57. R. Fernandez-Leiro, S. H. W. Scheres, A pipeline approach to single-particle processing in RELION. *Acta. Crystallogr. D. Struct. Biol.* **73**, 496–502 (2017).

58. R. Sanchez-Garcia, J. Gomez-Blanco, A. Cuervo, J. M. Carazo, C. O. S. Sorzano, J. Vargas, DeepEMhancer: A deep learning solution for cryo-EM volume post-processing. *Commun. Biol.* **4**, 874 (2021).

59. T. I. Croll, ISOLDE: A physically realistic environment for model building into low-resolution electron-density maps. *Acta. Crystallogr. D. Struct. Biol.* **74**, 519–530 (2018).

60. P. D. Adams, K. Gopal, R. W. Grosse-Kunstleve, L. W. Hung, T. R. Ioerger, A. J. McCoy, N. W. Moriarty, R. K. Pai, R. J. Read, T. D. Romo, J. C. Sacchettini, N. K. Sauter, L. C. Storoni, T. C. Terwilliger, Recent developments in the PHENIX software for automated crystallographic structure determination. *J. Synchrotron Radiat.* **11**, 53–55 (2004).